International Symposium
On Turbulence and Shear Flow
Phenomena (TSFP-8)
August 28 - 30, 2013 Poitiers, France

A LINEAR-NONLINEAR SEPARATION METHOD FOR DIRECT NUMERICAL SIMULATION OF SHOCK-TURBULENCE INTERACTION

X. Y. Hu and N. A. Adams
Lehrstuhl für Aerodynamik, Technische Universität München
85748 Garching, Germany
xiangyu.hu@tum.de

B. Wang
School of Aerospace, Tsinghua University
100084 Beijing, China

ABSTRACT

In this work, we propose a linear-nonlinear separation method, which hybridizes the 5th-order dispersion-dissipation-optimized WENO scheme in Hu *et al.* (2012) with its optimal linear scheme, for direct numerical simulation of shock-turbulence interaction. The method is based on the characteristic-wise formulation, by which the application of linear and nonlinear schemes are separated by measuring the non-resolvability of the linear scheme. Taking the advantage of characteristic-wise formulation, the measurement is formulated as a single universal non-dimensional number. Since the linear scheme omits the computation of the WENO weights, and most of the characteristic-projection operations, the scheme increase the overall computational efficiency greatly.

Introduction

In direct numerical simulation (DNS) of shock-turbulence interaction, there are three essential requirements for the choice of numerical schemes: high-order accuracy and low-dissipation to capture the fine-scale turbulent flow features, high numerical stability to capture flow discontinuities and as high as possible computational efficiency. However, it is very difficult to find a single numerical scheme which is able to meet all these requirements. On one hand, many linear schemes, including standard finite difference schemes and compact schemes, can achieve very high order of accuracy and very low numerical dissipation with high computational efficiency, but are not numerically stable when there are flow discontinuities. On the other hand, many nonlinear schemes, such as such as PPM, FCT, MUSCL and WENO, can achieve very high numerical stability and sufficient high-order accuracy, but have high numerical dissipation and low computational efficiency.

A promising approach to overcome these difficulties is using hybrid methods as in Refs. Adams & K. (1996); Johnsen *et al.* (2010); Pirozzoli (2011). The key idea is switching or blending between the nonlinear scheme and the linear scheme according to a shock sensor or discontinuity detector. The discontinuity detector is usually implement by the trouble-cell detecting approach, in which the numerical fluxes at cell-faces of all the neighboring cells are computed by the nonlinear scheme, or by the characteristic-wise approach, in which the discontinuity detectors are implemented on evaluating the numerical flux of each component on the characteristic filed. Up to now, the choice of an effective discontinuity detector remains a problematic issue for these methods when applied to complex or large-range of applications. Usually, problem-dependent parameters are required to tune for more stable simulation, more accurate results or higher computational efficiency.

In this paper, we propose a simple, highly efficient hybrid WENO scheme based on the characteristic-decomposition approach. The scheme switches the numerical fluxes of each characteristic variables between those of the WENO scheme and its corresponding optimal linear scheme. Since the linear scheme omits the computation of the WENO weights, and most of the characteristic-projection operations due to component-wise reconstruction, it increases the overall computational efficiency largely. Furthermore, the scheme employs a new broadly effective non-dimensional discontinuity detector, which measures the resolution limit of the linear scheme and does not degenerate at critical points.

Method

We assume that the fluid is inviscid and compressible, described by the one-dimensional Euler equations as

$$\frac{\partial \mathbf{U}}{\partial t} + \frac{\partial \mathbf{F}(\mathbf{U})}{\partial x} = 0, \tag{1}$$

where $\mathbf{U} = (\rho, m, E)^T$, and $\mathbf{F}(\mathbf{U}) = [m, \rho u^2 + p, (E+p)u]^T$. This set of equations describes the conservation laws for mass density ρ, momentum density $m \equiv \rho u$ and total energy density $E = \rho e + \rho u^2/2$, where e is the specific internal energy. To close this set of equations, the ideal-gas equation of state $p = (\gamma - 1)\rho e$ with a constant γ is used.

Characteristic-wise WENO scheme

For completeness, we briefly recall the classical 5th-order WENO scheme in Jiang & Shu (1996) for solving Eq. (1). The discretization is within the spatial domain such that $x_i = i\Delta x$, $i = 0,...,N$, where Δx is the spatial step, the semi-discretized form by the method of lines yields a system of ordinary differential equations

$$\frac{d\mathbf{U}_i}{dt} = \frac{1}{\Delta x}\left(\hat{\mathbf{F}}_{i-1/2} - \hat{\mathbf{F}}_{i+1/2}\right), \tag{2}$$

where $\hat{\mathbf{F}}_{i\pm1/2}$ are the numerical flux at $x_{i\pm1/2}$, respectively. Once the right-hand side of this expression has been evaluated, a TVD Runge-Kutta method is employed to advance the solution in time. In the typical characteristic-wise finite-difference WENO scheme, the $\hat{\mathbf{F}}_{i+1/2}$ are usually reconstructed within the local characteristic fields. Let us take the matrix $\mathbf{A}_{i+1/2}$ to be the Roe-average Jacobian $\partial\mathbf{F}/\partial\mathbf{U}$ at $x_{i+1/2}$. We denote by λ_s, $\mathbf{r}_s$ (column vector) and $\mathbf{l}_s$ (row vector) the sth eigenvalue, and the right and left eigenvectors of $\mathbf{A}_{i+1/2}$, respectively. The physical fluxes and conservative variables on the respective reconstruction stencil are mapped to the characteristic field by the characteristic-projection step

$$v_{j,s} = \mathbf{l}_s \cdot \mathbf{U}_j, \quad g_{j,s} = \mathbf{l}_s \cdot \mathbf{F}_j, \tag{3}$$

where $i+3 > j > i-2$ and $s = 1,2,3$. For each component of the characteristic variables, the corresponding split numerical fluxes are constructed by

$$f^+_{j,s} = \frac{1}{2}\left(g_{j,s} + \alpha_s v_{j,s}\right), \quad f^-_{j,s} = \frac{1}{2}\left(g_{j,s} - \alpha_s v_{j,s}\right), \tag{4}$$

where $\alpha_s = |\lambda_s|$ for a Roe flux (RF). Alternatively one can use $\alpha_s = \max|\lambda_{l,s}|$, where l represents the entire computational domain for a Lax-Friedrichs flux (LF) or the neighborhood of i for a local Lax-Friedrichs flux (LLF).

The calssical fifth-order WENO reconstruction in Jiang & Shu (1996) gives

$$f^+_{i+1/2,s} = \sum_{k=0}^{2} \omega^+_{k,s} f^+_{k,i+1/2}, \quad f^-_{i+1/2,s} = \sum_{k=0}^{2} \omega^-_{k,s} f^-_{k,i+1/2,s}, \tag{5}$$

where $f^\pm_{k,i\pm1/2,s}$ are 3rd-order reconstructions from the 3 upwind 3-point stencils, and $\omega^\pm_{k,s}$ are WENO weights defined by

$$\omega^\pm_{k,s} = \frac{\alpha_k}{\sum_{k=0}^{2}\alpha_{k,s}}, \quad \alpha_{k,s} = \frac{d_k}{(\beta_{k,s}+\varepsilon)^q}, \tag{6}$$

where $d_k = \{\frac{3}{10}, \frac{3}{5}, \frac{1}{10}\}$ are optimal weights. These optimal weights generate the 5th-order upwind scheme, by which the numerical flux is reconstructed from a 5-point stencil. $\varepsilon > 0$ prevents division by zero, $q = 1$ or 2 is chosen to adjust the distinct weights, and $\beta_{k,s}$ are the smoothness indicators. For the 5th-order dispersion-dissipation-optimized WENO scheme in Hu *et al.* (2012), the reconstruction uses all the 4 upwind and downwind 3-point stencils. The nonlinear weights are given by

$$\omega_k = \frac{\alpha_k}{\sum_{k=0}^{3}\alpha_k}, \quad \alpha_k = d_k\left(C_q + \frac{\tau_6}{\beta_{3,k}+\varepsilon\Delta x^2}\right)^q, \tag{7}$$

where $d_k = \{0.065, 0.495, 0.405, 0.035\}$ are the optimal weights yielding a low dissipation 5th-order linear scheme, $q = 4$ is an integer parameter, $C_q = 10^3$ is a positive constant parameter and $\varepsilon = 10^{-8}$ is a small positive number. For the WENO methodology and the details of computing $\beta_{3,r}$, $\beta_{3,ave}$ and τ_6, the reader should refer to Ref. Hu & Adams (2011).

The numerical flux in each characteristic field is then computed by

$$\hat{f}_{i+1/2,s} = f^+_{i+1/2,s} + f^-_{i+1/2,s}. \tag{8}$$

At last, this numerical flux is projected back to the physical space by

$$\hat{\mathbf{F}}_{i+1/2} = \sum_{s=1}^{3} \hat{f}_{i+1/2,s}\mathbf{r}_s. \tag{9}$$

It can be found that the major part of floating-point operations in the characteristic-wise WENO scheme are due to the characteristic-projection step (matrix-vector product) of Eq. (3), and the computation of the WENO weights in Eq. (6).

Hybrid WENO scheme

In order to decrease the number of floating-point operations, we propose to hybridize the WENO scheme with its optimal linear scheme by the characteristic-decomposition approach. A straightforward implementation is to switch between Eq. (8) and the corresponding flux of the optimal linear scheme based on the characteristic-variable projection. Here, however, we consider a component-wise reconstruction for the optimal linear scheme to further save the computational effort for the characteristic-projection step.

Optimal linear scheme with component-wise reconstruction In this formulation, the approximated physical fluxes and the differences of approximated conservative variables at $x_{i+1/2}$ are computed component-by-component as

$$\mathbf{F}_{i+1/2} = \frac{1}{2}\left(\mathbf{F}^+_{i+1/2} + \mathbf{F}^-_{i+1/2}\right), \tag{10}$$

$$\Delta\mathbf{U}_{i+1/2} = \frac{1}{2}\left(\mathbf{U}^+_{i+1/2} - \mathbf{U}^-_{i+1/2}\right). \tag{11}$$

With the optimal linear scheme of the 5th-order dispersion-dissipation-optimized WENO scheme, one has

$$\begin{aligned}\mathbf{F}_{i+1/2} = \frac{1}{60}(&\mathbf{F}_{i-2} - 8\mathbf{F}_{i-1} + 37\mathbf{F}_i \\ &+ 37\mathbf{F}_{i+1} - 8\mathbf{F}_{i+2} + \mathbf{F}_{i+3}),\end{aligned} \tag{12}$$

$$\begin{aligned}\Delta\mathbf{U}_{i+1/2} = \frac{1}{200}(&\mathbf{U}_{i-2} - 5\mathbf{U}_{i-1} + 10\mathbf{U}_i \\ &- 10\mathbf{U}_{i+1} + 5\mathbf{U}_{i+2} - \mathbf{U}_{i+3}).\end{aligned} \tag{13}$$

Note that Taylor-series expansion of Eq. (13) suggests

$$\Delta\mathbf{U}_{i+1/2} = -\frac{\Delta x^5}{200}\left.\frac{\partial^5\mathbf{U}(x)}{\partial x^5}\right|_{i+1/2} + O(\Delta x^7). \tag{14}$$

Then $\mathbf{F}_{i+1/2}$ and $\Delta\mathbf{U}_{i+1/2}$ are projected onto the characteristic field by

$$\Delta v_{i+1/2,s} = \mathbf{l}_s \cdot \Delta\mathbf{U}_{i+1/2}, \quad g_{i+1/2,s} = \mathbf{l}_s \cdot \mathbf{F}_{i+1/2}. \tag{15}$$

For each component of the characteristic variables, the corresponding numerical flux is constructed by

$$\hat{f}_{i+1/2,s} = g_{i+1/2,s} + \alpha_s \Delta v_{i+1/2,s}, \tag{16}$$

where α_s are chosen in the same way as Eq. (4). At last, the numerical flux obtained in each characteristic field is projected back to the component space by Eq. (9). Note that, compared to the characteristic-wise WENO scheme, the linear scheme omits the computation of the WENO weights in Eq. (6), and decreases by $5/6$ the characteristic-projection operations of Eq. (3).

Hybridization and discontinuity detector

Since the linear scheme is numerically unstable for solutions with discontinuities, it should be switched on only in smooth regions of the solution according to a discontinuity detector. A proper discontinuity detector should rely on problem-independent measure to indicate that the resolution limit of the linear scheme is reached. A usual way to achieve a problem-independent measure is using the non-dimensional ratio between high- and low order undivided differences, like in Refs. Ren *et al.* (2003); Kim & Kwon (2005); Li & Qiu (2010). Since undivided difference corresponds to approximation of a spatial derivative, this type of discontinuity detectors degenerate near critical points with zero low order derivatives as the denominators approach zero and switches on the WENO scheme. To decrease the over-dissipation associated with the degeneration, dimensional parameters must be introduced, which lead again to problem-dependent discontinuity detectors.

In this paper, we achieve a problem-independent measure in a different way. By noticing that the characteristic variables have the dimension of density we define a non-dimensional discontinuity detector by

$$\sigma_s = \left(\frac{\Delta v_{i+1/2,s}}{\tilde{\rho}} \right)^2, \tag{17}$$

where $\tilde{\rho}$ is the Roe-average density of $\mathbf{A}_{i+1/2}$. From Eq. (14) it can be found that σ_s also is related to the 5th-order derivatives of the characteristic variables due to the linearized characteristic projection. Since the optimal 5th-order linear scheme reconstructs with 4th-degree polynomials and is not able to resolve 5th or higher order derivatives, σ_s is actually a measure on the resolution limit of the linear scheme. If there is no vacuum in the flow (which is almost always the case), the denominator of σ_s does not degenerate.

With a given threshold $\varepsilon \ll 1$, the hybrid scheme can be constructed as follows: for each component of the characteristic variables the numerical flux is obtained by linear flux of Eq. (16) if $\sigma_s < \varepsilon$; otherwise it is obtained by WENO flux of Eq. (8). Note that the above approach can be directly applied to multiple dimensions by a dimension-by-dimension approach, and can be very easily extended to higher-order or modified WENO schemes. The only modification for other WENO schemes is that Eq. (10) should be computed with the corresponding optimal linear schemes.

Numerical examples

The following numerical examples are provided to illustrate the potential of the proposed hybrid WENO scheme. The governing equations are the one- and two-dimensional compressible Euler or Navier-Stokes equations. While the original 5th-order dispersion-dissipation-optimized WENO scheme is denoted as WENO-5, the present hybrid scheme is denoted as H-WENO-5. The 3rd-order TVD Runge-Kutta scheme is used for time integration as in Shu & Osher (1989). The local computational efficiency on each cell-face through the entire computation time is measured by $\eta = M_{Linear}/(M_{Linear} + M_{WENO})$, where M_{WENO} is the number of operations with WENO flux and M_{Linear} is the number of operations with linear flux. The overall computational efficiency is obtained by averaging η over the entire computational domain. We set $\varepsilon = 10^{-7}$ for all numerical examples. If not mentioned otherwise, all the computations are carried out with a CFL number of 0.6.

Propagation of broadband sound waves

This problem, taken from Sun *et al.* (2011), corresponds to the propagation of a sound wave packet which contains acoustic turbulent structure with various length scales. The initial condition is

$$\begin{aligned}
p(x,0) &= p_0 \left\{ 1 + \varepsilon \sum_{k=1}^{N/2} \left[E_p(k) \right]^{1/2} \sin\left[2\pi k (x + \phi_k) \right] \right\}, \\
\rho(x,0) &= \rho_0 \left[\frac{p(x,0)}{p_0} \right]^{1/\gamma}, \\
u(x,0) &= u_0 + \frac{2}{\gamma - 1} \left[\frac{c(x,0)}{c_0} \right],
\end{aligned}$$

where ϕ_k is a random number between 0 and 1 with uniform distribution, $\varepsilon = 10^{-3}$, $\gamma = 1.4$, c is the speed of sound and

$$E_p(k) = \left(\frac{k}{k_0} \right)^4 \exp^{-2(k/k_0)^2}$$

is the energy spectrum which reaches its maximum at $k = k_0$. A periodic boundary condition is applied at $x = 0$ and $x = 1$. Computations have been carried out on a 128-point grid using a CFL number of 0.2 for one period of time. The numerical results shown in Fig. 1 suggest that no WENO flux is switched on during the computation and the solution recovers that obtained by the optimal linear scheme.

Shock interaction problems

Here, we consider two important shock interaction problems: the shock-density-wave interaction problem from Shu & Osher (1989) and the two-blast-wave interaction problem from Colella & Woodward (1984).

For the shock density-wave interaction problem, the initial condition is set by a Mach 3 shock interacting with a perturbed density field

$$(\rho, u, p) = \begin{cases} (3.857, 2.629, 10.333) & \text{if } 0 \le x < 1 \\ (1 + 0.2\sin(5x), 0, 1) & \text{if } 10 \ge x > 1 \end{cases}$$

and the final time is $t = 1.8$. A zero-gradient boundary condition is applied at $x = 0$ and 10. We examine the numerical

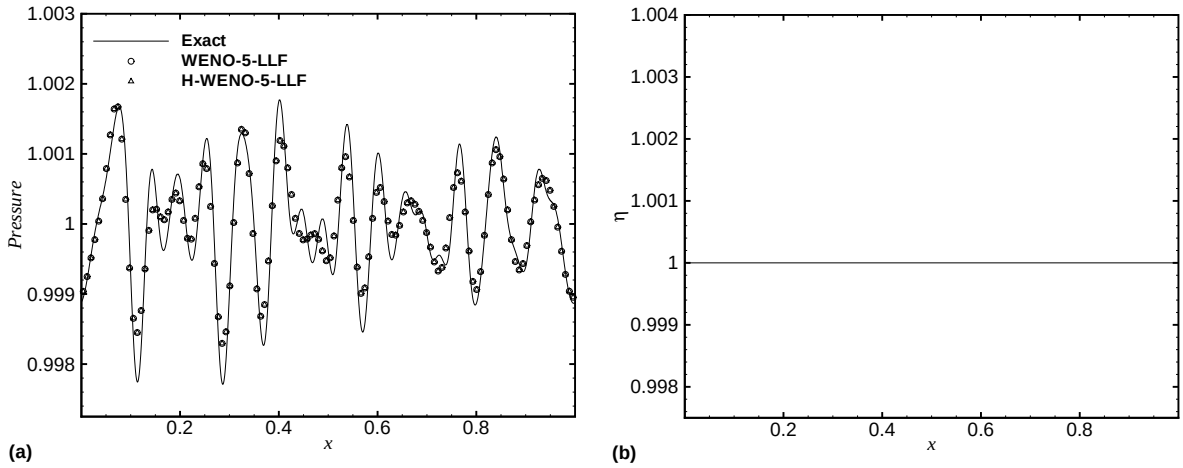

Figure 1. Propagation of broadband sound waves computed on a 128 points grid: (a) pressure and (b) local computational efficiency distribution.

solution on a 200-point grid. For the two-blast-wave interaction problem, the initial condition is

$$(\rho,u,p)=\begin{cases}(1,0,1000) & \text{if } 0<x<0.1\\ (1,0,0.01) & \text{if } 0.1<x<0.9\\ (1,0,100) & \text{if } 1>x>0.9\end{cases},$$

and the final time is $t=0.038$. The reflective boundary condition is applied at both $x=0$ and $x=1$. We examine the numerical solution on a 400-point grid. Nothe that, the reference "exact" solutions for this two problems are the high-resolution solutions on a 3200-point grid computed by WENO-CU6 scheme from Hu *et al.* (2010).

Figure 2 gives the profiles of computed density and local computational efficiency. While good agreement with the reference solutions is observed, and the overall efficiencies of 97.7% and 91.9%, respectively, are obtained. Note that, while producing numerical stable solution for the two-blast-wave interaction problem, the present method achieves solutions of comparable or better accuracy than previous hybrid schemes in Refs. Johnsen *et al.* (2010); Adams & K. (1996) for shock-density wave interaction problem.

Viscous shock tube problem

We consider the two-dimensional viscous flow problem in a square shock tube with unit height and insulated walls from Daru & Tenaud (2000). In this problem, the propagation of the incident shock wave and contact discontinuity lead to a thin boundary layer. After its reflection on the right wall, the shock wave interacts with this boundary layer and results a separation region and the formation of a typical "λ-shape like shock pattern". The initial condition is

$$(\rho,u,p)=\begin{cases}(120,0,120/\gamma) & \text{if } 0\le x<\frac{1}{2}\\ (1.2,0,1.2/\gamma) & \text{if } 1\ge x>\frac{1}{2}\end{cases}$$

The fluid is assumed as ideal gas with $\gamma=1.4$ and constant dynamics viscosity $\mu=0.005$ and Prandtl number $Pr=0.73$ and satisfying the Stokes assumption. If the reference values are chosen as the initial speed of sound, unit density and unit length, the Reynolds number is 200. By applying the symmetry condition at the upper boundary, only the lower half domain is actually computed. For other boundaries, the no-slip and adiabatic wall conditions are applied. The viscous and heat transfer is calculated by 6th-order accuracy, Here, we examine the numerical solution with two resolutions on a grid of 500×250 points.

Figure 3 gives the profiles of computed density and local computational efficiency. Note that, numerical convergence is indicated because no notable differences, except the near shock region, can be identified from the converged density contours in Sjögreen & Yee (2003) obtained with much higher grid resolutions. Also note that the overall efficiency for this problem is 99.4%, which suggests essentially negligible effort for computing WENO flux.

Concluding remarks

We propose a simple hybrid WENO scheme to increase computational efficiency and decrease numerical dissipation. Based on the characteristic-wise approach, the scheme switches the numerical flux of each characteristic variables between that of the WENO scheme and its optimal linear scheme according to a discontinuity detector measuring the resolution limit of the linear scheme. As shown by a number of numerical examples the overall efficiency, measured by the fraction of linear flux used, is always higher than 90%, shows that the hybridization increases the computational efficiency largely. Also, by choosing the largely problem-independent threshold for the discontinuity detector, compared to the original WENO scheme, much lower overall numerical dissipation is achieved without compensating robustness. Since the method uses a general characteristic-wise formulation of the WENO scheme, it can be applied to multiple-species flows, where the overhead of local characteristic projection and WENO weights calculation is even more serious.

REFERENCES

Adams, N.A. & K., Shariff 1996 A high-resolution hybrid compact-ENO scheme for shock-turbulence interaction

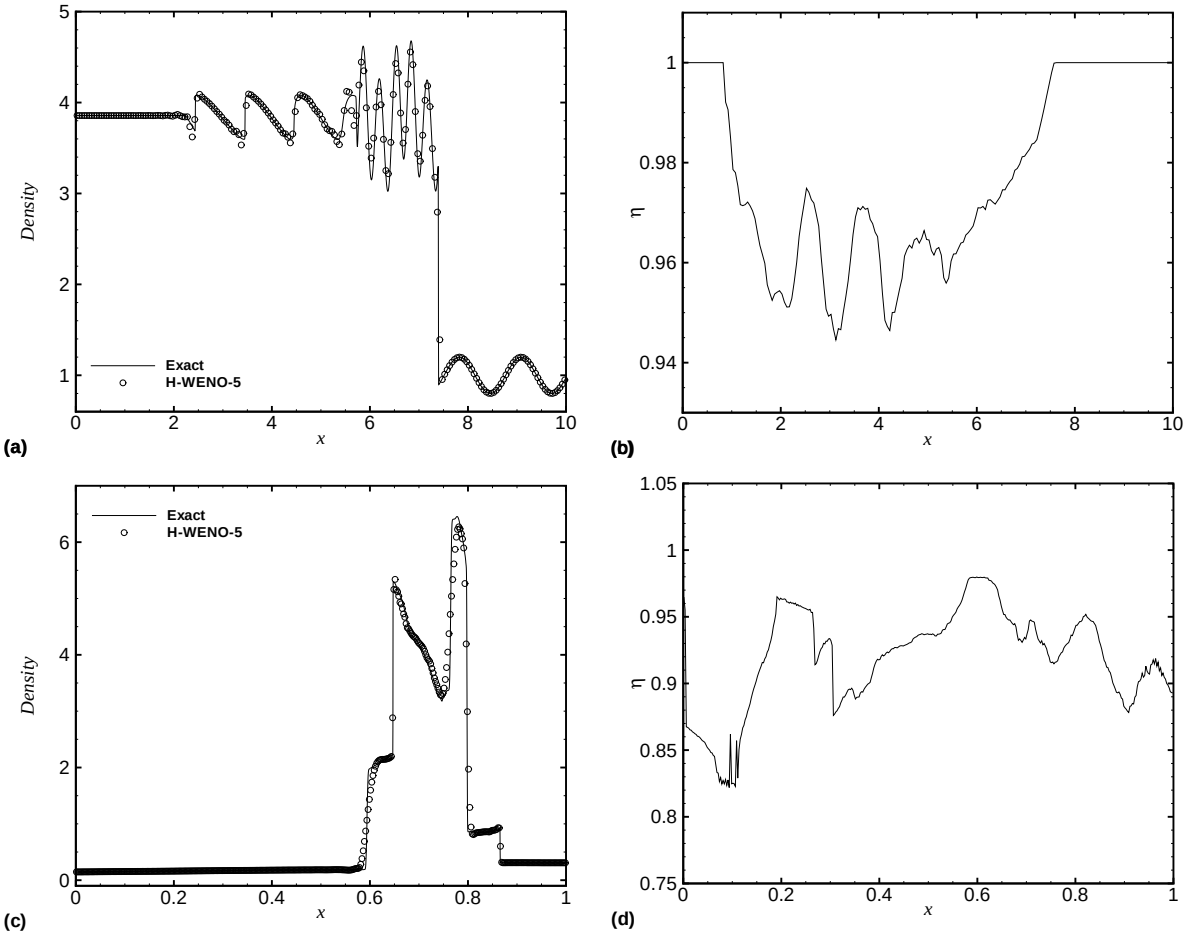

Figure 2. one-dimensional examples: (a) density and (b) local computational efficiency for the shock-density-wave interaction problem computed on 200 grid points; (c) density and (d) local computational efficiency for the two-blast-wave interaction problem computed on 400 grid points.

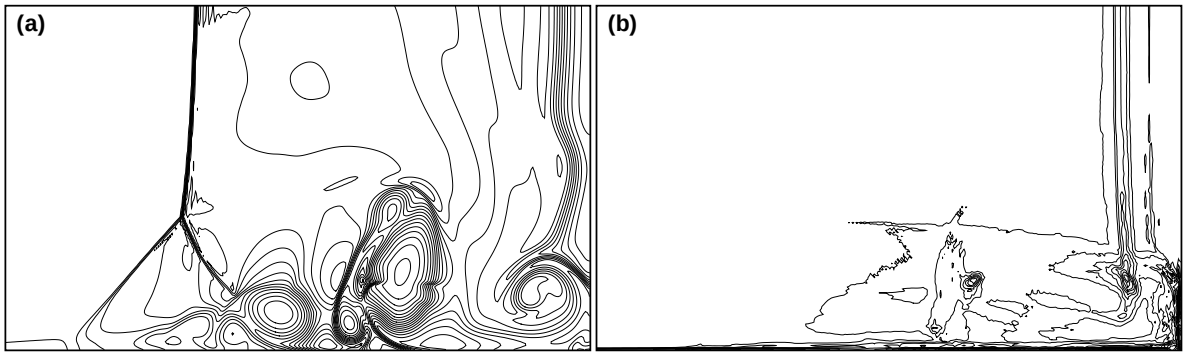

Figure 3. Viscous shock-tube problem computed on 500×250 grid points: (a) 20 density contours from 15 to 130, (b) 20 local computational efficiency contours from 0.81 to 0.99.

problems. *J. Comput. Phys.* **127**, 27–51.

Colella, P. & Woodward, P.R. 1984 The Piecewise Parabolic Method (PPM) for gas-dynamical simulations. *J. Comput. Phys.* **54** (1), 174–201.

Daru, V. & Tenaud, C. 2000 Evaluation of tvd high resolution schemes for unsteady viscous shocked flows. *Computers & fluids* **30** (1), 89–113.

Hu, XY & Adams, NA 2011 Scale separation for implicit large eddy simulation. *J. Comput. Phys.* **230** (19), 7240–7249.

Hu, XY, Pirozzoli, S & Adams, NA 2012 Dispersion-dissipation condition for finite difference schemes. *arXiv*

preprint arXiv:1204.5088 .

Hu, X.Y., Wang, Q. & Adams, N.A. 2010 An adaptive central-upwind weighted essentially non-oscillatory scheme. *J. Comput. Phys.* **229** (23), 8952–8965.

Jiang, G.S. & Shu, C.W. 1996 Efficient implementation of weighted ENO schemes. *J. Comput. Phys* **126**, 202–228.

Johnsen, E., Larsson, J., Bhagatwala, A.V., Cabot, W. H., Moin, P., Olson, B. J., Rawat, P. S., Shankar, S. K., Sjögreen, B., Yee, H.C., Zhong, X. & Lele, S. K. 2010 Assessment of high-resolution methods for numerical simulations of compressible turbulence with shock waves. *J. Comput. Phys.* **229** (4), 1213–1237.

Kim, D. & Kwon, J.H. 2005 A high-order accurate hybrid scheme using a central flux scheme and a weno scheme for compressible flowfield analysis. *J. Comput. Phys.* **210** (2), 554–583.

Li, G. & Qiu, J. 2010 Hybrid weighted essentially non-oscillatory schemes with different indicators. *J. Comput. Phys.* **229** (21), 8105–8129.

Pirozzoli, S. 2011 Numerical methods for high-speed flows. *Ann. Rev. Fluid Mech.* **43**, 163–194.

Ren, Y.X., Liu, M. & Zhang, H. 2003 A characteristic-wise hybrid compact-weno scheme for solving hyperbolic conservation laws. *J. Comput. Phys.* **192** (2), 365–386.

Shu, C.W. & Osher, S. 1989 Efficient implementation of essentially non-oscillatory shock-capturing schemes, II. *J. Comput. Phys.* **83** (1), 32–78.

Sjögreen, B. & Yee, HC 2003 Grid convergence of high order methods for multiscale complex unsteady viscous compressible flows. *J. Comput. Phys.* **185** (1), 1–26.

Sun, Zhen-Sheng, Ren, Yu-Xin, Larricq, Cédric, Zhang, Shi-ying & Yang, Yue-cheng 2011 A class of finite difference schemes with low dispersion and controllable dissipation for dns of compressible turbulence. *J. Comput. Phys.* **230** (12), 4616–4635.